DRAFT VERSION JULY 15, 2019
Preprint typeset using LaTeX style emulateapj v. 08/22/09

SHEAR-CURRENT EFFECT IN MAGNETIZED BURGULENCE

MAARIT J. KÄPYLÄ, MATTHIAS RHEINHARDT, AXEL BRANDENBURG, NISHANT SINGH, PETRI KÄPYLÄ

Subject headings:

1. INTRODUCTION

In addition to all other experiments we have made to study the possibility of the magnetic shear current effect, we have now developed a closer connection to the work of Squire and Bhattacharjee. Squire (in an email after the Tokyo MPPC meeting) made a concrete proposal to try to reproduce their Fig 9 in Squire & Bhattacharjee (2015), which is attempted here.

In this figure they show cases where they use both kinetic and magnetic forcing of variable strengths in a box with an aspect ratio of 8 with a shear parameter S=1 and forcing wave number of $k_{\rm f}$=3. They state that the resulting $u_{\rm rms}$ in their purely kinematically forced model is 0.2, and the magnetic Reynolds number is roughly five. This corresponds to a shear number ${\rm Sh}_{\rm K}=-1.7$ using our definition. So far none of our models have such large shear numbers, hence a completely new set of runs had to be performed to match their results.

2. MODELS USED

As we do not have the compressible test-field method yet in a state of full production, we have to adopt a cumbersome step-by-step approach. The test-field method currently available for the magnetically forced case is the non-linear test-field method that utilises simplified MHD equations. Hence, we first need to establish how the simplified MHD compares with the full MHD in the quasi-kinematic regime (that is, without magnetic forcing), by utilizing the quasi-kinematic test-field method on these runs. At our final step, we then switch on magnetic forcing, and utilize the simplified non-linear test-field in the limit of simplified MHD, and compare how the results change in between kinetic and magnetic forcing. The systems of equations and test field methods are briefly described in the appendix.

3. RESULTS

In all cases, be it full or simplified MHD, the first instability to be excited is the generation of patchy flows in the horizontal velocity components. These are most likely signatures of the vorticity dynamo (see, Elperin et al. 2003; Käpylä et al. 2009); it is unclear whether in Squire & Bhattacharjee (2015) such flows were present or not. In any case, they have a very strong effect on the dynamics and especially on the solutions of the test problems (cause instabilities). Therefore we need to suppress these mean (xy-averaged) flows artificially.

3.1. *Kinetically forced full MHD case*

The first studied case is a full MHD (FK8*) runs with kinetic forcing. We aim for ${\rm Sh}_{\rm K}$ and ${\rm Re}_{\rm M}$ matching as closely as possible to those of Squire & Bhattacharjee (2015). We initialise the magnetic field with Gaussian noise of the amplitude 10^{-10}. As seen in Figure 1 rightmost columns, the radial (x) component undergoes an exponential decay, while the azimuthal (y) component is first enhanced until 40 turnover times. After that, however, it will start decaying with the same exponential rate as the radial component. It undergoes some occasional burst-like enhancement episodes, very often seen in sheared systems due to the tangling caused by the shear flow, but the overall trend remains decaying. Looking at the individual Fourier modes (lower left panels of Figure 1) one sees that all except one Fourier mode (k_zL_z=1), at the largest scale of the box, show a decaying trend. The slower decay of the smallest allowed wavenumber may be explained by diffusion acting slowest on it; hence we do not interpret this being the dynamo solution eigenmode that would appear when the dynamo would be supercritical.

To see the real dynamo eigenmode, we perform an additional run, Run FK8b, with somewhat larger magnetic Reynolds number (by lowering the magnetic diffusivities). The results are shown in Figure 2. In this run, indeed, we see an exponential growth, both in the rms values of the horizontally averaged fields, but also in the individual large-scale Fourier modes, with radial and azimuthal components having identical growth rates. The dominating mode in the azimuthal field spectrum is k_zL_z=9, and we regard this as the wavenumber of the dynamo instability in this system.

Next we turn into the measurements of the turbulent transport coefficients, to try to explain what is driving the dynamo in this system. We use the quasi-kinematic test-field method, which behaves here very well with stable test solutions that saturate into a plateau, and the measurement of the turbulent transport coefficients can be done reliably. We recover the standard result of large, positive η_{xy}, and a much smaller, positive η_{yx}, see Table 1. The diagonal elements of the diffusivity tensor are positive and about equally big. We also measure the rms-values of the α tensor coefficients, to check for the possibility of an incoherent α shear-effect in the system. As the presence of shear-current effect requires negative values of η_{yx} (see Appendix D), the cause of the dynamo in the system cannot be this effect. This is not a new result, and has been already obtained by many authors. The remaining candidate is the α-shear dynamo; we have computed the dynamo numbers $D_{\alpha S}$ for this instability (see Appendix E), and measure subcritical values for the Run FK8a, while clearly supercritical values for the Run FK8b. The dynamo eigenmode is relatively close to the forcing scale, which further supports this dynamo of being of this type.

3.2. *Kinetically forced simplified MHD case of "Magnetized Burgulence"*

Next we repeat the same experiment with the simplified MHD setup with kinetic forcing only (SK8a). This is to bridge the way to the non-linear test-field method that currently only works with the simplified MHD equations. This time we find an exponentially growing dynamo (although the growth is really slow), both radial and azimuthal rms mean field components exhibiting the same growth rate, see Figure 3. The scale of the excited mean magnetic fields is $k_zL_z=2$, the radial and azimuthal Fourier mode time evolutions being shown with thick blue lines in Figure 3. Two things are worth noting immediately: here, dynamo growth is obtained with identical parameters to the Run FK8a, that was not dynamo-active, and

TABLE 1
SUMMARY OF THE RUNS. ALL OF THEM HAVE k_f=5, $\nu = 10^{-2}$, $\eta = 3 \times 10^{-3}$ (FK, SK1,SMx), $\eta 2 \times 10^{-3}$ (SK2), $\eta = 5 \times 10^{-4}$ (SK3), AND $S = -0.25$.

Run	$\mathrm{Sh_K}$	$\mathrm{Re_M}$	Lu	η_{xx}/η	η_{yy}/η	η_{xy}/η	η_{yx}/η	$\alpha_{\rm rms}$	$k_z L_z$	$D_{\eta S}$	$D_{\alpha S}$
FK8a	-1.6	2.1	1(-10)	0.402 ± 0.008	0.396 ± 0.007	0.265 ± 0.008	0.033 ± 0.001	0.037	9*	-0.5	1.1
FK8b	-1.6	12.7	3(-8)	2.557 ± 0.108	2.521 ± 0.103	1.784 ± 0.118	0.095 ± 0.005	0.219	9	-3.0	6.1
SK1a	-1.6	2.1	0.0	0.241 ± 0.003	0.264 ± 0.004	0.193 ± 0.004	-0.007 ± 0.000	0.074	1	0.4	3.9
SK1b	-1.6	12.8	9(-6)	1.782 ± 0.015	1.888 ± 0.022	1.778 ± 0.040	-0.067 ± 0.003	0.692	1	4.2	43.0
SK1c	-1.6	13.0	1.6	1.758 ± 0.053	1.875 ± 0.053	1.747 ± 0.088	-0.067 ± 0.004	0.691	1	4.1	43.4
SK4a	-1.5	2.2	1(-10)	0.241 ± 0.002	0.262 ± 0.003	0.191 ± 0.007	-0.007 ± 0.000	0.037	3	0.7	4.6
SK4b	-1.5	13.0	2(-7)	1.774 ± 0.010	1.864 ± 0.012	1.744 ± 0.040	-0.073 ± 0.002	0.342	4	4.6	21.4
SK4c	-0.7	1.9	9(-11)	0.262 ± 0.004	0.269 ± 0.004	0.080 ± 0.003	-0.007 ± 0.001	0.039	3	0.2	2.6
SK8a	-1.6	2.2	1(-8)	0.245 ± 0.002	0.266 ± 0.002	0.196 ± 0.004	-0.007 ± 0.000	0.052	2	6.0	94.4
SK8b	-1.6	12.9	2(-4)	1.800 ± 0.016	1.892 ± 0.010	1.776 ± 0.029	-0.071 ± 0.003	0.25	8	4.4	15.2
SK8c											
SKM1a	-1.8	1.9	4.6	0.168 ± 0.003	0.191 ± 0.006	0.178 ± 0.004	-0.009 ± 0.000	0.066	1	0.5	3.9
SKM1b	-1.3	15.9	40.5	2.839 ± 0.191	3.340 ± 0.249	2.923 ± 0.288	-0.196 ± 0.014	1.227	1	5.8	36.7
SKM1c	-0.9	1.6	4.3	0.185 ± 0.008	0.191 ± 0.008	0.084 ± 0.009	-0.007 ± 0.001	0.059	1	0.2	1.4
SKM4a	-1.5	2.3	4.9	0.264 ± 0.022	0.316 ± 0.027	0.306 ± 0.019	-0.015 ± 0.001	0.056	1	12.2	180.1
SKM4b	-1.3	15.2	40.0	2.659 ± 0.250	3.024 ± 0.345	2.582 ± 0.471	-0.187 ± 0.025	0.574	1	101.5	1244.8
SKM4c											
SM8a	-1.6	2.1	4.7	0.221 ± 0.045	0.261 ± 0.059	0.252 ± 0.060	-0.013 ± 0.003	0.036	1	44.0	1005.9
SM8b											
SM8c											
SKM8a	-1.9	1.7	4.6	0.198 ± 0.029	0.237 ± 0.039	0.240 ± 0.051	-0.012 ± 0.002	0.025	2	11.1	89.6
SKM8b	-1.3	16.0	41.0	2.864 ± 0.311	3.331 ± 0.481	2.979 ± 0.679	-0.198 ± 0.028	0.428	2	93.1	794.1
SKM8c	-0.9	1.5	4.3	0.192 ± 0.014	0.199 ± 0.018	0.092 ± 0.014	-0.006 ± 0.001	0.020	2	2.4	30.1
SKM16a	-1.5	2.3	5.0	0.258 ± 0.018	0.305 ± 0.020	0.289 ± 0.014	-0.015 ± 0.000	0.028	3	20.6	211.6
SKM16b											
SKM16c											

that the scale of the generated field here is considerably larger. This already hints that maybe the same dynamo mechanisms are not at play in these two systems.

We again apply the quasi-kinematic test-field method, and find well-behaved test solutions, similarly to the full MHD case. The sign of η_{yx} is now negative and the diagonal elements of $\boldsymbol{\eta}$ are nearly ten times smaller than in the full MHD cacse, see Table 1. When we consider the dynamo numbers $D_{\eta S}$ and $D_{\alpha S}$ for the shear-current and incoherent α shear dynamo instabilities, respectively, we see that both dispersion relations predict dynamo action, and hence, based on this run alone, it is difficult to judge which dynamo instability would be in operation here.

Therefore, we perform some additional runs, SK1 and SK4 inspecting the sensitivity of the system to its vertical size. Run SK1 is a cubic box of the dimensions of 2π, whilst SK4 has an aspect ratio of four. In the former system, no dynamo develops, but all field components and individual Fourier components decay. Again, the slowest to decay is the box-scale $k_z L_z$ component that can persist quite some time in this strongly sheared system. Run SK4 shows close to marginal dynamo action similar to Run FK8a, with radial modes showing exponential decay at all times, while azimuthal component first shows enhancement, which is closer to being linear than exponential, but then after some time an eventual decay occurs. The vertical scale of the eigenmode is close to that in Run SK8a. Hence, the dynamo instability is strongly dependent on the vertical box size, hinting towards the box having to be large enough to capture the growing dynamo mode. The measured turbulent transport coefficients in these three runs, only varying by their vertical extent, are nearly identical, as expected, further giving credibility to this hypothesis. The dispersion relations indicate that the system should be sub-, slightly sub, and clearly supercritical for the shear-current effect, while supercritical to the incoherent α- shear effect in all of SK1, SK4, and SK8a, respectively. We have also performed some additional runs with varying magnetic Reynolds number, which shows that the growth rate of the instability is enhanced with growing Rm. With all this evidence at hand, we conclude that the dynamo seen in the magnetized Burgulence setup is most likely a shear-current dynamo effect.

3.3. *Magnetically forced simplified MHD cases; "Doubly magnetic Burgulence"*

Finally, we switch to magnetic forcing of the same magnitude as the kinetic forcing. (thus corresponding to Fig. 9d of SC15), and use the nonlinear test-field method. We again perform several runs with varying vertical extent of the box, and also vary the magnetic Reynolds number.

In all the Runs, the magnetic forcing (in a few turnover times) quickly generates a superequipartition magnetic field. From this point onwards, the radial and azimuthal mean rms fields and their individual Fourier components behave differently than in the two previous setups investigated. We do not see distinguishable exponential growth in the azimuthal nor in the radial fields, and the growth/decay rates of the different field components are different. The azimuthal component undergoes similar, erratic, "activity bursts" than seen in the other types of setups as well, their frequency depending on the vertical box scale. In the cubic 2π run of SKM1, see Figure 4, the outburst frequency is high, and the generated structures fill in the whole domain vertically. The outbursts get less and less frequent in SKM4 (see Figure 5), SKM8 (see Figure 5) and SKM16 (see Figure 5), and the structures are more long lived. In none of the cases, however, any signs of dynamo instability can be distinguished. In all cases except SKM16, which

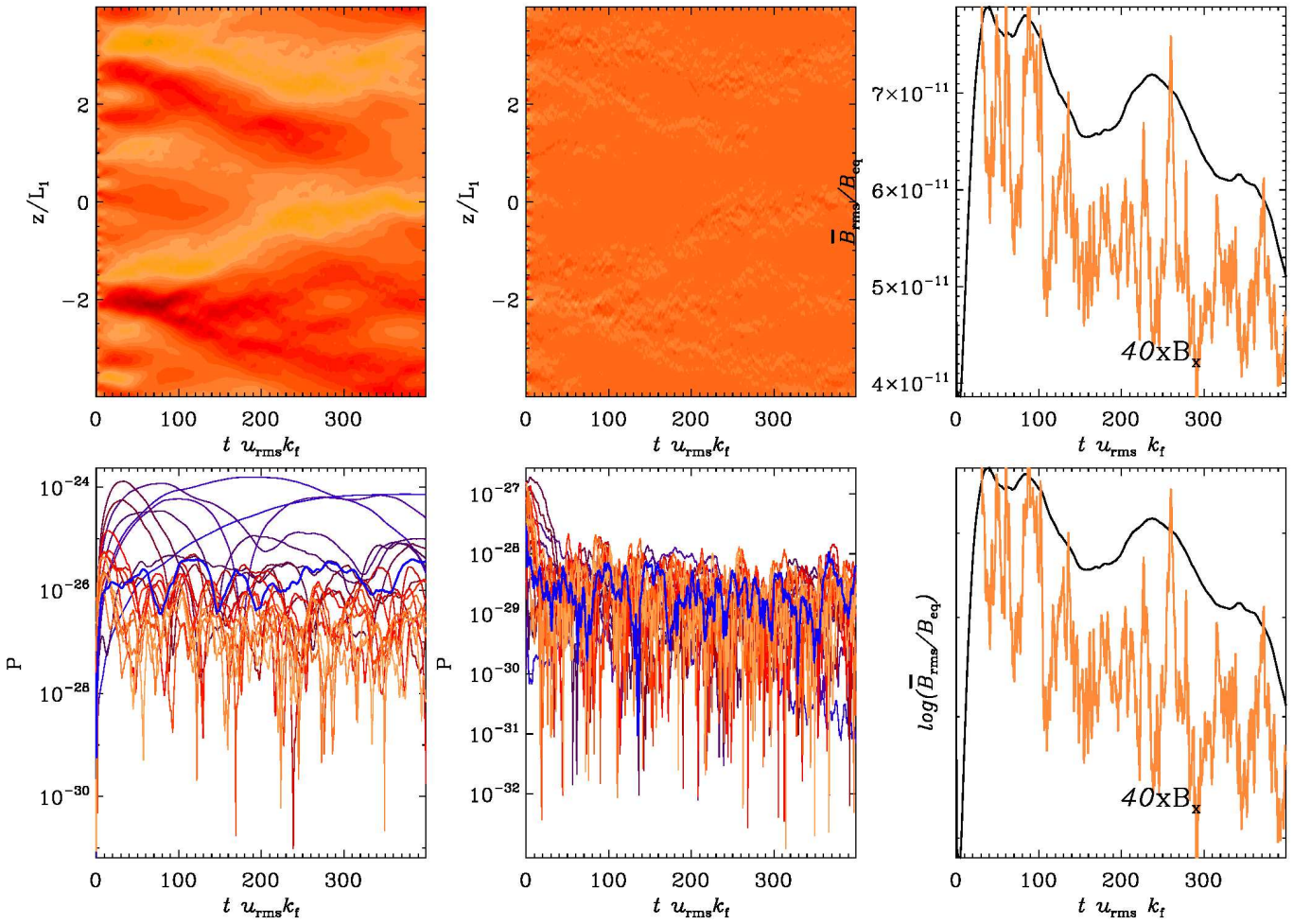

FIG. 1.— Horizontally averaged magnetic fields as function of time (upper left azimuthal, upper middle radial component), the time evolution of the mean rms fields computed from these averages (top right, linear scale; bottom right, logarithmic scale), and the time evolution of the individual twenty smallest Fourier modes (lower left for azimuthal component; lower middle for the radial component). Time is measured in turnover times. The rms values of the radial component has been enhanced by 40 times. In the plot for the Fourier modes, increasingly blue color indicates smaller wavenumbers, increasingly red higher wavenumbers. The thick line indicates the Fourier mode where the fastest growing mode ($k_z L_z$=9) is obtained in a run with a supercritical dynamo (FK8b).

may be due to the fact that it has not been run long enough, the final field configuration is volume filling. We interpret this as the action of the shear, tangling the magnetic fluctuations provided by the continuous forcing, and diffusion acting as erasing the smaller scales more rapidly than the larger ones.

The measurement of the turbulent transport coefficients does not reveal any dramatic changes in any of the coefficients due to setting the magnetic forcing on. Also the purely magnetically forced Run SM8 yields coefficients of the same magnitude and sign as its purely kinematically or kinetically-magnetically forced cases of the same aspect ratio. Inspecting the dispersion relations, even though it is not meaningful in the case of any of the magnetically forced cases, as no dynamo instabilities (pre-requisite for using these formulae) are found, reveals that both dynamo effects should be present nearly in all the systems investigated. The only case where the dynamo coefficient for the magnetic shear current effect is less than one (subcritical) is Run SKM1, which shows the generation of coherent volume-filling structures in the same way as all the other runs. Hence, the magnetically forced runs cannot be interpreted in the framework of mean-field dynamo effects.

4. CONCLUSIONS

We have studied different types of sheared MHD systems with the quasi-kinematic (QKTFM) and simplified non-linear (NLTFM) test-field methods. In the case of full MHD equations studied with the we confirm the evidence for dynamo action owing to the incoherent α shear effect. In magnetized Burgulence, perhaps only an academically interesting simplification of the MHD equations (neglecting the pressure gradient term from the Navier Stokes equation), but the only system that can currently be studied with the NLTFM, we observe a sign change of the η_{yx} component, that can be theoretically shown to enable the shear-current effect driven dynamos. Indeed, dynamo action is found, and its properties and excitation conditions match those of expected from the shear-current effect theory. In the case of the recently frequently studied systems with magnetic forcing, we do not find any signatures of dynamo action (no exponential growth of the magnetic field components, the radial and azimuthal components showing different, non-exponential behavior), nor a signifi-

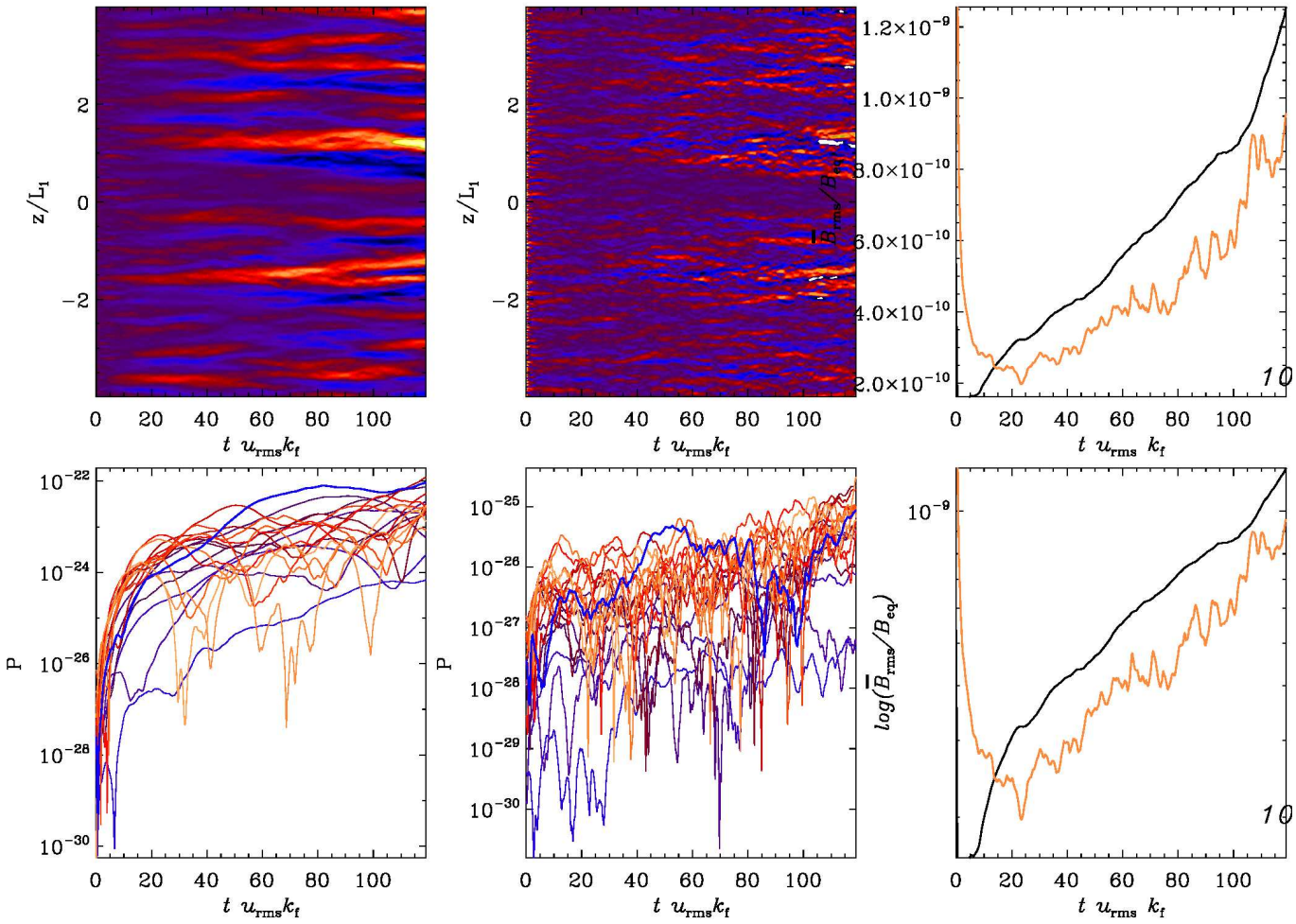

FIG. 2.— The same as Figure 1, but the thick line in the lower leftmost panels indicates the dominant Fourier mode generated by the dynamo, namely ($k_z L_z$=9).

cant change in any of the turbulent transport coefficients when compared to their kinetically forced counterparts. On the contrary, the generated coherent large-scale structures could be due to the tangling of the magnetic fluctuations by the strong shear. We conclude that the magnetically forced cases cannot be interpreted in the framework of mean-field dynamo theory.

REFERENCES

Squire, J., & Bhattacharjee, A. 2015, ApJ, 813, 52

Brandenburg, A., Rädler, K.-H., Rheinhardt, M., & Käpylä, P. J. 2008a, ApJ, 676, 740

Elperin, T., Kleeorin, N. & Rogachevskii, I. 2003, Phys. Rev. E, 68, 016311

Käpylä, P. J., Mitra, D., & Brandenburg, A. 2009, Phys. Rev. E, 79, 016302

Rheinhardt, M., & Brandenburg, A. 2010, A&A, 520, A28 (RB10)

Yousef, T. A., Heinemann, T., Schekochihin, A. A., Kleeorin, N., Rogachevskii, I., Iskakov, A. B., Cowley, S. C., & McWilliams, J. C. 2008, Phys. Rev. Lett., 100, 184501

APPENDIX

A. SMHD

The equations of SMHD, as defined here, are similar to those of MHD, but without the pressure gradient in the momentum equation. Correspondingly, the density ρ is held constant. So we have

$$\mathcal{D}^A \boldsymbol{A} = \boldsymbol{U}\times\boldsymbol{B} + \boldsymbol{F}_{\rm M} + \eta\nabla^2\boldsymbol{A}, \tag{A1}$$

$$\mathcal{D}^U \boldsymbol{U} = -\boldsymbol{U}\cdot\nabla\boldsymbol{U} + \boldsymbol{J}\times\boldsymbol{B}/\rho + \boldsymbol{F}_{\rm K} + \nu(\nabla^2\boldsymbol{U} + \nabla\nabla\cdot\boldsymbol{U}/3) \tag{A2}$$

with the linear expressions

$$\mathcal{D}^A \boldsymbol{A} = (\partial_t + Sx\partial_y)\boldsymbol{A} + S\hat{\boldsymbol{x}}A_y, \tag{A3}$$

$$\mathcal{D}^U \boldsymbol{U} = (\partial_t + Sx\partial_y + 2\boldsymbol{\Omega}\times)\boldsymbol{U} + S\hat{\boldsymbol{y}}U_x. \tag{A4}$$

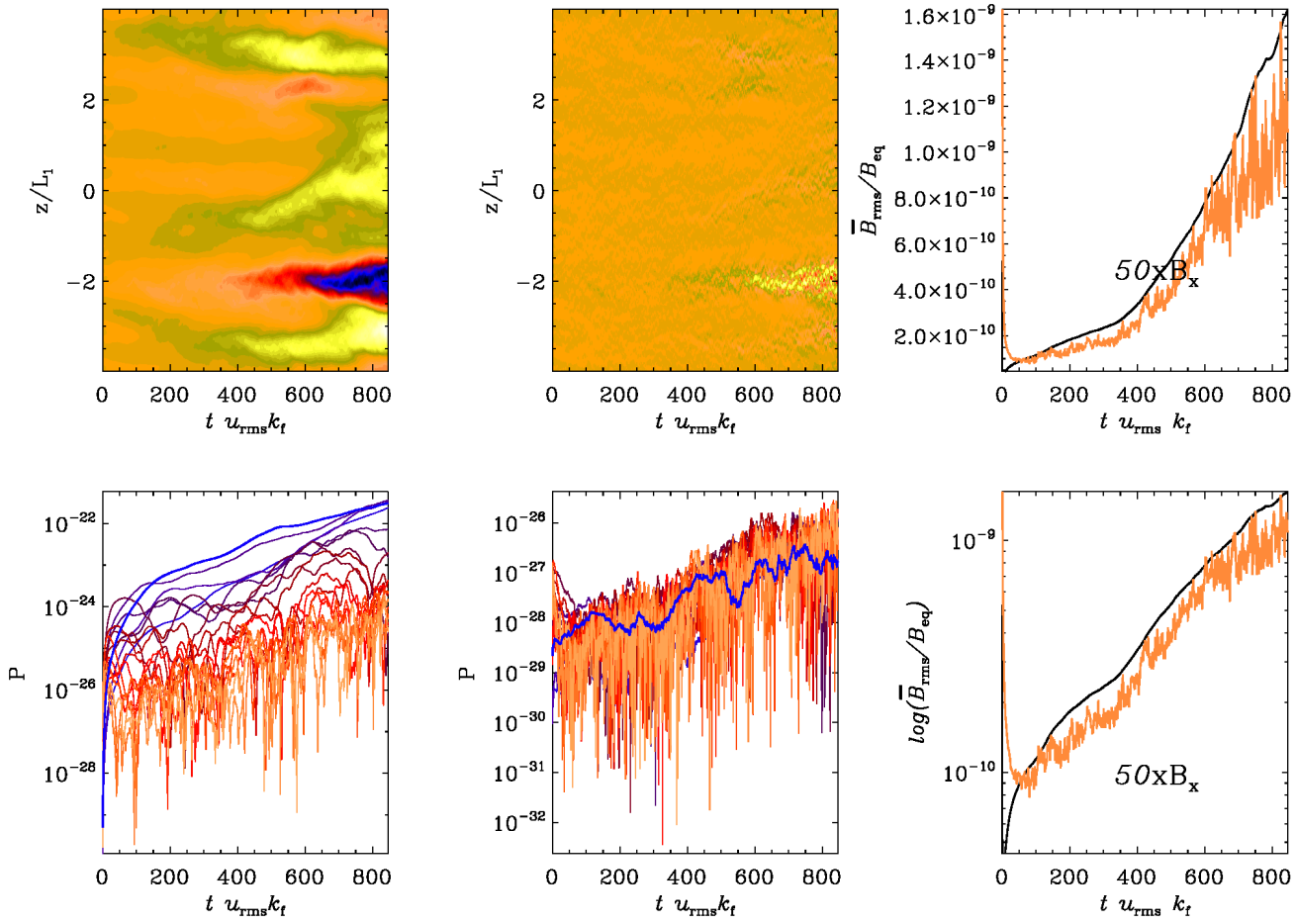

FIG. 3.— The same as Figure 2, but for Run SK8a.

$\boldsymbol{B} = \boldsymbol{\nabla} \times \boldsymbol{A}$ is the magnetic field, $\boldsymbol{J} = \boldsymbol{\nabla} \times \boldsymbol{B}$ is the current density in units where the vacuum permeability is unity, $\boldsymbol{F}_{\rm K}$ and $\boldsymbol{F}_{\rm M}$ are kinetic and magnetic forcing functions, respectively, $\boldsymbol{U}$ is the velocity, η is the magnetic diffusivity, and ν is the kinematic viscosity, both considered constant.

The main advantage of using SMHD is to avoid the necessity of dealing with density fluctuations and corresponding effects in the mean quantities. As self-advection $\boldsymbol{U} \cdot \nabla \boldsymbol{U}$ is no longer discarded, we are here more general than Rheinhardt & Brandenburg (2010) (hereafter, RB10) which, in physical terms, suffered from the implied assumption of slow fluid motions, that is, Strouhal number St $\ll 1$ or Re $\ll 1$. Moreover, a complete neglect of the self-advection term is inadequate in the present context given that shear plays its essential role just via this term. So merely the terms arising from an additional mean flow (apart from the shear flow $\overline{\boldsymbol{U}}^S$) and that by the fluctuating velocity, $\boldsymbol{u} \cdot \nabla \boldsymbol{u}$ could all be neglected. The latter neglect, however, would be equivalent to restrict the method to SOCA w.r.t. to the self-advection term which is not desirable.

B. NLTFM

In situation with shear, a complication in applying mean-field concepts based on the horizontal average arises from the fact, that, for linear shear, in general $\overline{\boldsymbol{U}^S} \neq \boldsymbol{U}^S$ (when defined to be $\propto x$ the mean even vanishes) whereas $\partial_i U_j^S$ is spatially constant, hence a pure mean.

The evolution equations for the fluctuations in the magnetic vector potential, $\boldsymbol{a} = \boldsymbol{A} - \overline{\boldsymbol{A}}$, and the velocity, $\boldsymbol{u} = \boldsymbol{U} - \overline{\boldsymbol{U}}$, follow

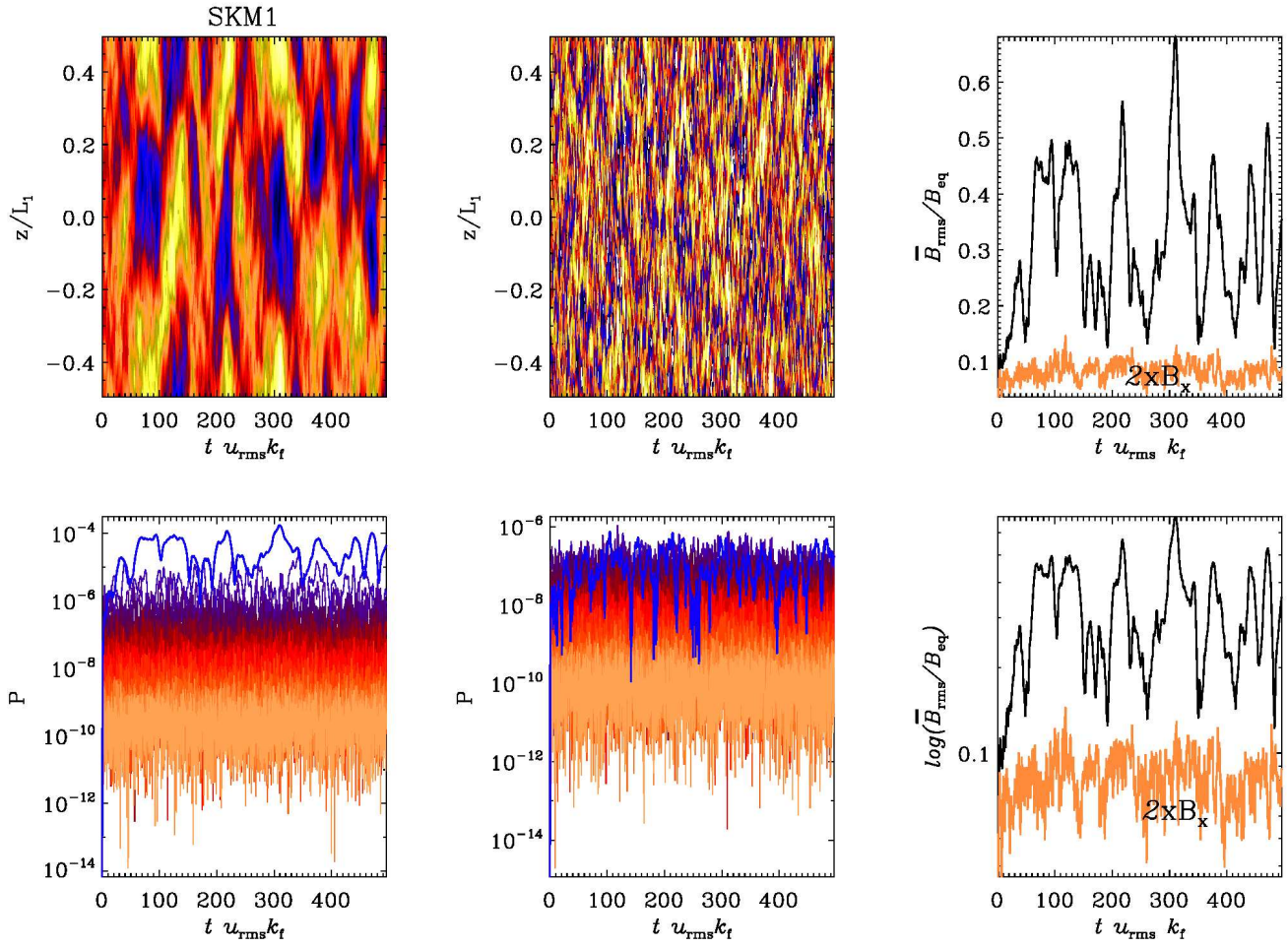

FIG. 4.— The same as Figure 2, but for Run SKM1.

from Equations (A1) and (A2) as

$$\mathcal{D}^A \boldsymbol{a} = \overline{\boldsymbol{U}} \times \boldsymbol{b} + \boldsymbol{u} \times \overline{\boldsymbol{B}} + (\boldsymbol{u} \times \boldsymbol{b})' + \boldsymbol{f}_{\rm K} + \eta \nabla^2 \boldsymbol{a}, \tag{B1}$$

$$\mathcal{D}^U \boldsymbol{u} = \left(\overline{\boldsymbol{J}} \times \boldsymbol{b} + \boldsymbol{j} \times \overline{\boldsymbol{B}} + (\boldsymbol{j} \times \boldsymbol{b})'\right)/\rho + \boldsymbol{f}_{\rm M} \tag{B2}$$

$$+(\boldsymbol{u} \cdot \nabla \boldsymbol{u})' + \overline{\boldsymbol{U}} \cdot \nabla \boldsymbol{u} + \boldsymbol{u} \cdot \nabla \overline{\boldsymbol{U}} \tag{B3}$$

$$+\nu(\nabla^2 \boldsymbol{u} + \nabla \nabla \cdot \boldsymbol{u}/3),$$

where fluctuations are either denoted by lowercase symbols, or by primes like $(\boldsymbol{u} \times \boldsymbol{b})' = \boldsymbol{u} \times \boldsymbol{b} - \overline{\boldsymbol{u} \times \boldsymbol{b}}$, etc.

We solve these equations not by setting $\overline{\boldsymbol{B}}$ to the actual mean field resulting from the solutions of Equations (A1) and (A2), but rather with $\overline{\boldsymbol{B}}$ from a set of test fields, $\boldsymbol{B}^{\rm T}$, namely

$$\boldsymbol{B}^1 = (\cos kz, 0, 0), \quad \boldsymbol{B}^2 = (\sin kz, 0, 0), \tag{B4}$$

$$\boldsymbol{B}^3 = (0, \cos kz, 0), \quad \boldsymbol{B}^4 = (0, \sin kz, 0), \tag{B5}$$

where k is the wavenumber of the test field, being a multiple of $2\pi/L_z$. From the solutions of Equations (B1) and (B2) we can construct the mean electromotive force, $\overline{\boldsymbol{\mathcal{E}}} = \overline{\boldsymbol{u} \times \boldsymbol{b}}$ and the mean ponderomotive force, $\overline{\boldsymbol{\mathcal{F}}} = \overline{\boldsymbol{j} \times \boldsymbol{b}}$, which are then expressed in terms of the mean field by the ansatzes

$$\overline{\mathcal{E}}_i = \alpha_{ij} \overline{B}_j - \eta_{ij} \overline{J}_j, \tag{B6}$$

$$\overline{\mathcal{F}}_i = \phi_{ij} \overline{B}_j - \psi_{ij} \overline{J}_j. \tag{B7}$$

where i, j adopt only the values $1, 2$ as a consequence of setting the anyway constant $\overline{B}_z$ arbitrarily to zero. Hence, each of the four tensors, α_{ij}, η_{ij}, ϕ_{ij}, ψ_{ij}, has four components, i.e., altogether we have 16 unknowns.

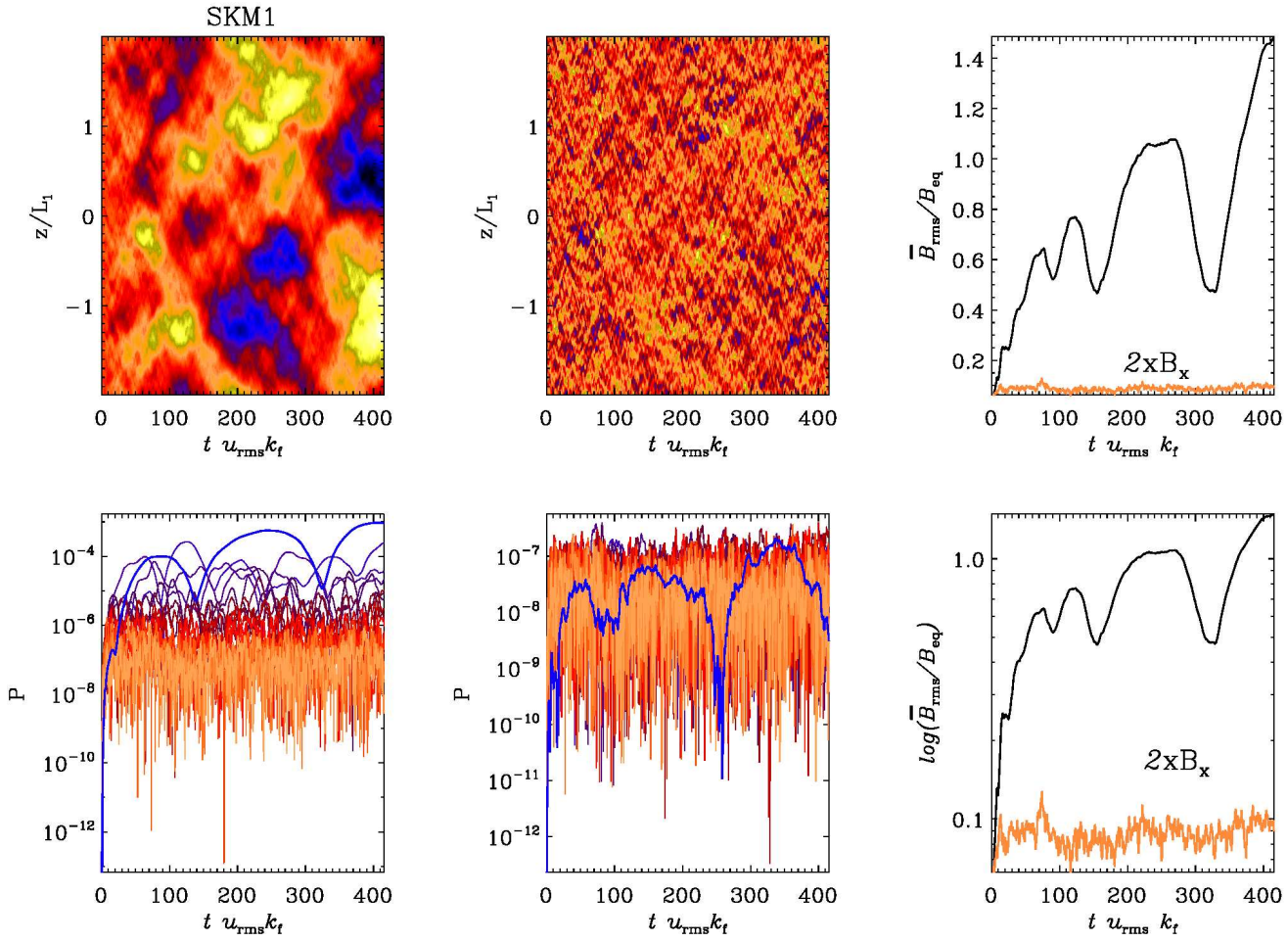

FIG. 5.— The same as Figure 2, but for Run SKM4.

In the QKTFM, $\overline{\boldsymbol{\mathcal{E}}}$, considered as a functional of $\boldsymbol{u}$, $\overline{\boldsymbol{U}}$, and $\overline{\boldsymbol{B}}$, is linear in $\overline{\boldsymbol{B}}$. In the more general case with a magnetic background turbulence, this is a priori no longer the case. To deal with this difficulty, RB10 added the evolution equations for the background turbulence, that is, the turbulence in the absence of the mean field, ($\boldsymbol{u}_0$, $\boldsymbol{b}_0$) which are similar to Equations (B1) and (B2), but for zero mean field, to the equations of the TFM. In general, $\overline{\boldsymbol{\mathcal{E}}}$ can be split into a contribution $\overline{\boldsymbol{u}_0 \times \boldsymbol{b}_0}$ that is independent of the mean field and a contribution

$$\overline{\boldsymbol{\mathcal{E}}}_{\bar{\boldsymbol{B}}} = \overline{\boldsymbol{u}_0 \times \boldsymbol{b}_{\bar{\boldsymbol{B}}}} + \overline{\boldsymbol{u}_{\bar{\boldsymbol{B}}} \times \boldsymbol{b}_0} + \overline{\boldsymbol{u}_{\bar{\boldsymbol{B}}} \times \boldsymbol{b}_{\bar{\boldsymbol{B}}}}, \tag{B8}$$

where $\boldsymbol{u}_{\bar{\boldsymbol{B}}}$ and $\boldsymbol{b}_{\bar{\boldsymbol{B}}}$ denote those parts of the solutions of Equations (B1) and (B2) which are supposed to vanish for vanishing $\overline{\boldsymbol{B}}$. Using $\boldsymbol{u} = \boldsymbol{u}_0 + \boldsymbol{u}_{\bar{\boldsymbol{B}}}$ and $\boldsymbol{b} = \boldsymbol{b}_0 + \boldsymbol{b}_{\bar{\boldsymbol{B}}}$, $\overline{\boldsymbol{\mathcal{E}}}_{\bar{\boldsymbol{B}}}$ can be written in two equivalent ways as

$$\overline{\boldsymbol{\mathcal{E}}}_{\bar{\boldsymbol{B}}} = \overline{\boldsymbol{u} \times \boldsymbol{b}_{\bar{\boldsymbol{B}}}} + \overline{\boldsymbol{u}_{\bar{\boldsymbol{B}}} \times \boldsymbol{b}_0} = \overline{\boldsymbol{u}_0 \times \boldsymbol{b}_{\bar{\boldsymbol{B}}}} + \overline{\boldsymbol{u}_{\bar{\boldsymbol{B}}} \times \boldsymbol{b}}. \tag{B9}$$

Both become linear in quantities with subscript $\overline{\boldsymbol{B}}$ when $\boldsymbol{b}$ and $\boldsymbol{u}$ are identified with the fluctuating fields in the main run. In this way, we have recovered the mentioned linearity property of $\overline{\boldsymbol{\mathcal{E}}}[\overline{\boldsymbol{B}}]$ in the QKTFM. Likewise, one writes the part of the mean ponderomotive force $\overline{\boldsymbol{\mathcal{F}}}$, which results from the Lorentz force as

$$\overline{\boldsymbol{j} \times \boldsymbol{b}_{\bar{\boldsymbol{B}}}} + \overline{\boldsymbol{j}_{\bar{\boldsymbol{B}}} \times \boldsymbol{b}_0} = \overline{\boldsymbol{j}_0 \times \boldsymbol{b}_{\bar{\boldsymbol{B}}}} + \overline{\boldsymbol{j}_{\bar{\boldsymbol{B}}} \times \boldsymbol{b}}\,; \tag{B10}$$

and that resulting from self-advection as

$$\overline{\boldsymbol{u} \cdot \nabla \boldsymbol{u}_{\bar{\boldsymbol{B}}}} + \overline{\boldsymbol{u}_{\bar{\boldsymbol{B}}} \cdot \nabla \boldsymbol{u}_0} = \overline{\boldsymbol{u}_0 \cdot \nabla \boldsymbol{u}_{\bar{\boldsymbol{B}}}} + \overline{\boldsymbol{u}_{\bar{\boldsymbol{B}}} \cdot \nabla \boldsymbol{u}}\,; \tag{B11}$$

see Equations (29) and (30) of RB10. Corresponding expressions can be established for the fluctuating parts of the bilinear terms, $(\boldsymbol{u} \times \boldsymbol{b})'$, $(\boldsymbol{j} \times \boldsymbol{b})'$ and $(\boldsymbol{u} \cdot \nabla \boldsymbol{u})'$. We recall that the different formulations of the fluctuating parts, obtained this way, result in

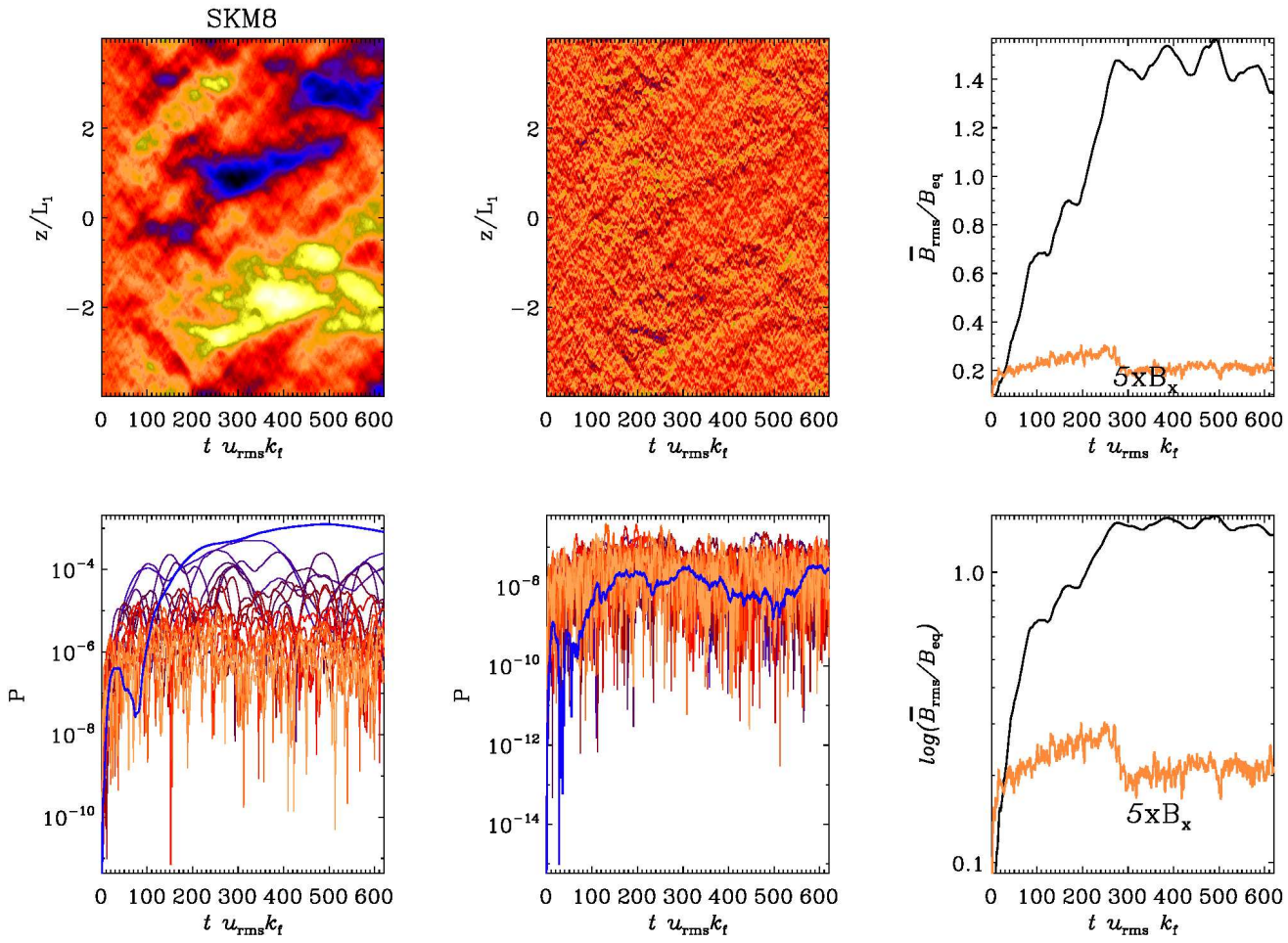

FIG. 6.— The same as Figure 2, but for Run SKM8.

different stability properties of the test problems. Here we chose to use in each of them the first formulation, resulting in what is called the "ju method"; see Table 1 of RB10.

C. QKTFM

We now state here for comparison the governing equations for the QKTFM. They consist of just Equation (B1), but not Equation (B2), and Equation (B6). Then Equation (B9) reduces simply to

$$\overline{\boldsymbol{\mathcal{E}}}_{\bar{\boldsymbol{B}}} = \overline{\boldsymbol{u} \times \boldsymbol{b}_{\bar{\boldsymbol{B}}}}. \quad \text{(QKTFM)}. \tag{C1}$$

Obviously, the contribution $\overline{\boldsymbol{u}_{\bar{\boldsymbol{B}}} \times \boldsymbol{b}_0}$ is missing. Again, for further details see RB10.

D. DISPERSION RELATION FOR SHEAR-CURRENT EFFECT DRIVEN DYNAMOS

For shear-current driven dynamos, the dispersion relation from the linear stability analysis for exponentially growing solutions reads (see e.g. Brandenburg et al. 2008)

$$\frac{\lambda_\pm}{\eta_T k_z^2} = -1 \pm \frac{1}{\eta_T} \sqrt{\left(\frac{S}{k_z^2} + \eta_{xy}\right) \eta_{yx} + \epsilon^2}, \tag{D1}$$

where $\eta_T = \eta + \eta_t$, $\eta_t = \frac{1}{2}(\eta_{xx} + \eta_{yy})$, and $\epsilon = \frac{1}{2}(\eta_{xx} - \eta_{yy})$. A necessary and sufficient condition for exponentially growing solutions is that the term in the square root is positive, and that it is larger than η_T^2. In other words (for $\epsilon \approx 0$, holding within the error limits for the measured diagonal elements of η)

$$D_{\eta S} \equiv \left(\frac{S}{k_z^2} + \eta_{xy}\right) \frac{\eta_{yx}}{\eta_T^2} > 1. \tag{D2}$$

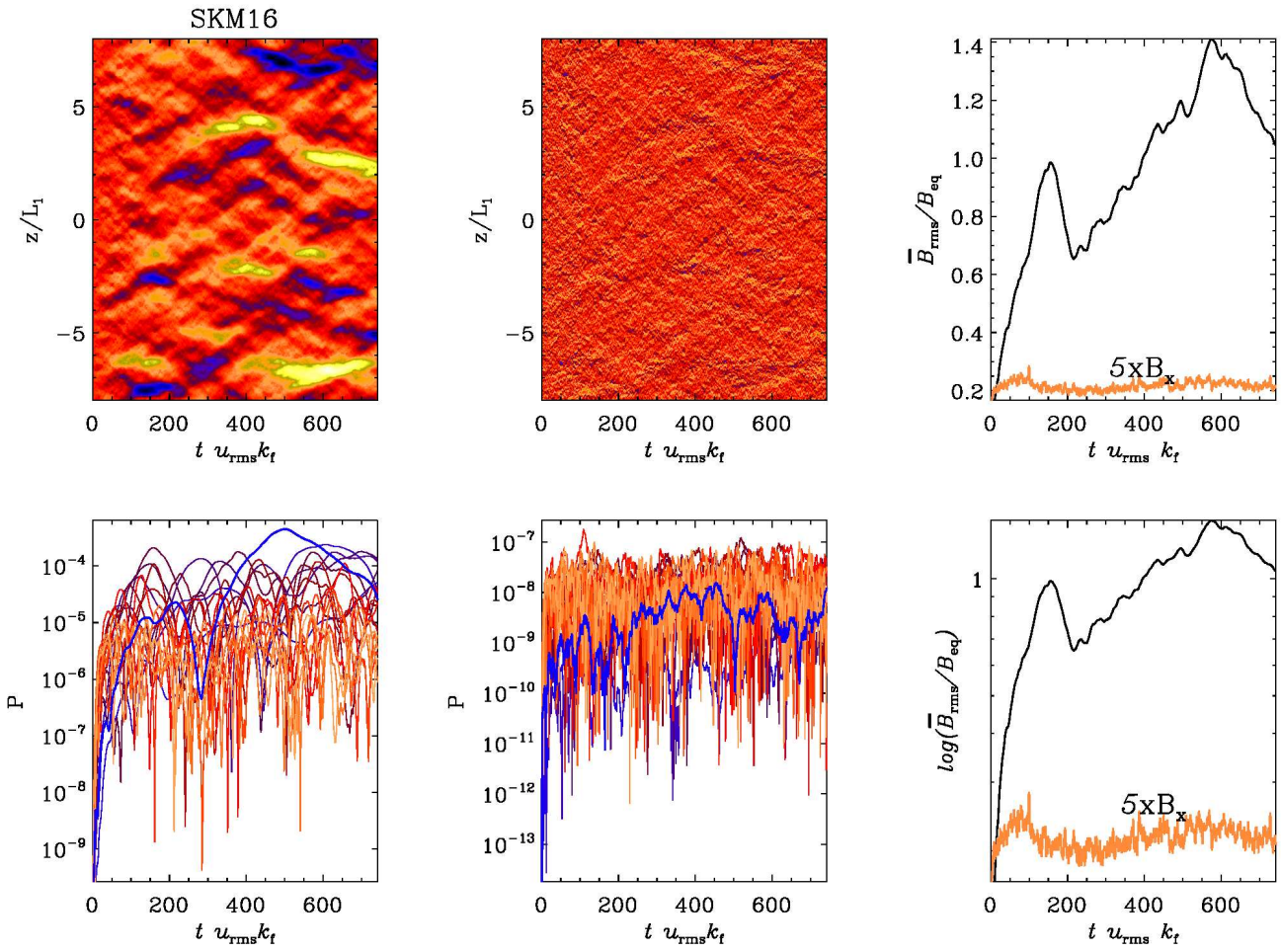

FIG. 7.— The same as Figure 2, but for Run SKM16.

We note here that the contribution from η_{xy} is sometimes not included in the excitation condition, as its effect is smaller than that coming from the first term. This also holds for systems studied here, but we note that, in general, η_{xy} is clearly non-zero, positive, and its magnitude is much larger than that of η_{yx}, hence setting it to zero, as is customary in some fitting experiments to determine the turbulent transport coefficients, is not justified.

E. DISPERSION RELATION FOR INCOHERENT SHEAR-α DYNAMOS

For incoherent α -shear driven dynamos, the dispersion relation from the linear stability analysis for exponentially growing solutions reads (see e.g. Brandenburg et al. 2008)

$$D_{\alpha S} = \frac{\alpha_{\rm rms}\,|S|}{\eta_T^2 k_z^3}, \tag{E1}$$

where the rms fluctuations of the α_{yy} component are usually accounted for. (see e.g. Brandenburg et al. 2008) derived the critical $D_{\alpha S}$ of approximately 2.3 for white-noise α effect.